



# Plasmonic enhancement of second-harmonic generation of dielectric layer embedded in metal-dielectric-metal structure

Kang, Byungjun  
Imakita, Kenji  
Fujii, Minoru  
Hayashi, Shinji

---

**(Citation)**

Journal of Applied Physics, 123(12):123103-123103

**(Issue Date)**

2018-03-28

**(Resource Type)**

journal article

**(Version)**

Version of Record

**(Rights)**

© 2018 Author(s). This article may be downloaded for personal use only. Any other use requires prior permission of the author and AIP Publishing. The following article appeared in Journal of Applied Physics 123(12), 123103 and may be found at <http://dx.doi.org/10.1063/1.5018239>

**(URL)**

<https://hdl.handle.net/20.500.14094/90006729>



# Plasmonic enhancement of second-harmonic generation of dielectric layer embedded in metal-dielectric-metal structure

Cite as: J. Appl. Phys. **123**, 123103 (2018); <https://doi.org/10.1063/1.5018239>

Submitted: 05 December 2017 . Accepted: 18 March 2018 . Published Online: 28 March 2018

Byungjun Kang, Kenji Imakita, Minoru Fujii , and Shinji Hayashi 



View Online



Export Citation



CrossMark

## ARTICLES YOU MAY BE INTERESTED IN

**Effect of layer number and metal-chloride dopant on multiple layers of graphene/porous Si solar cells**

Journal of Applied Physics **123**, 123101 (2018); <https://doi.org/10.1063/1.5013169>

**Line shape engineering of sharp Fano resonance in Al-based metal-dielectric multilayer structure**

Journal of Applied Physics **122**, 163103 (2017); <https://doi.org/10.1063/1.5002715>

**Efficient frequency conversion by combined photonic-plasmonic mode coupling**

Journal of Applied Physics **123**, 103101 (2018); <https://doi.org/10.1063/1.5017010>

Lock-in Amplifiers  
Find out more today



 Zurich  
Instruments



# Plasmonic enhancement of second-harmonic generation of dielectric layer embedded in metal-dielectric-metal structure

Byungjun Kang,<sup>1</sup> Kenji Imakita,<sup>1</sup> Minoru Fujii,<sup>1</sup> and Shinji Hayashi<sup>1,2,a)</sup>

<sup>1</sup>Department of Electrical and Electronic Engineering, Graduate School of Engineering, Kobe University, Kobe 657-8501, Japan

<sup>2</sup>Optics and Photonics Center, Moroccan Foundation for Science, Innovation and Research (MAScIR), Rabat 10100, Morocco

(Received 5 December 2017; accepted 18 March 2018; published online 28 March 2018)

The enhancement of second-harmonic generation from a dielectric layer embedded in a metal-dielectric-metal structure upon excitation of surface plasmon polaritons is demonstrated experimentally. The metal-dielectric-metal structure consisting of a  $\text{Ge}_x(\text{SiO}_2)_{1-x}$  layer sandwiched by two Ag layers was prepared, and the surface plasmon polaritons were excited in an attenuated total reflection geometry. The measured attenuated total reflection spectra exhibited two reflection dips corresponding to the excitation of two different surface plasmon polariton modes. Strong second-harmonic signals were observed under the excitation of these surface plasmon polariton modes. The results demonstrate that the second-harmonic intensity of the  $\text{Ge}_x(\text{SiO}_2)_{1-x}$  layer is highly enhanced relative to that of the single layer deposited on a substrate. Under the excitation of one of the two surface plasmon polariton modes, the estimated enhancement factor falls in a range between 39.9 and 171, while under the excitation of the other surface plasmon polariton mode, it falls in a range between 3.96 and 84.6. *Published by AIP Publishing.*

<https://doi.org/10.1063/1.5018239>

## I. INTRODUCTION

Since the first investigation of enhanced second-harmonic generation (SHG) in silver films reported by Simon, Mitchell, and Watson,<sup>1</sup> SHG enhancements mediated by excitations of surface plasmon polariton (SPP) modes propagating at metal-dielectric (MD) interfaces and those mediated by localized surface plasmon modes in metallic nanostructures have been the subject of extensive theoretical and experimental studies over the past decades. As described in recent review papers,<sup>2,3</sup> such SHG enhancements are nowadays discussed in the realm of nonlinear plasmonics, and a variety of potential applications have been suggested. Although the SHG enhancements have been observed successfully in plasmonic nanostructures, fabrication of the nanostructures is not always easy and is time consuming, preventing realistic applications. The quest for simpler plasmonic structures that are capable of enhancing SHG signals still remains a challenge.

One of the candidates for simpler plasmonic structures is a planar metal-dielectric-metal (MDM) structure that can be prepared without the nanofabrication technique. The dispersion relations of the SPP modes in the MDM structure have been studied theoretically early in 1969 by Economou.<sup>4</sup> In the MDM structure, coupling between two SPP modes propagating at inner MD and dielectric-metal (DM) interfaces results in a symmetric SPP (S-SPP) mode and an anti-symmetric SPP (A-SPP) mode.<sup>5,6</sup> When the M layers are thin and the structure is surrounded by dielectric mediums, the structure also supports SPP modes propagating at the outer MD interfaces. Under the excitation of these SPP modes, electric fields near the M surfaces are enhanced, offering the

opportunities for SHG enhancement of the M layers and layers adjacent to the M layers. Indeed, Teshima *et al.*<sup>7</sup> have succeeded in observing the SHG enhancement in the MDM structure consisting of a poly(methyl methacrylate) (PMMA) layer sandwiched by two Au layers under excitation of the S-SPP mode. Since the PMMA layer is SHG-inactive, the observed enhanced SHG signals come from the Au layers. As we have demonstrated for fluorescence signals using a dye layer embedded in the middle D layer in a MDM structure,<sup>8</sup> linear and nonlinear optical signals originating from the middle D layer can be enhanced upon excitations of the SPP modes. However, experimental evidence for the enhancement of SHG signals originating from the middle D layer has not yet been reported. The potential of the MDM structure for enhanced spectroscopies has not yet been fully explored.

In this paper, we report results of SHG measurements performed for MDM structures consisting of a  $\text{Ge}_x(\text{SiO}_2)_{1-x}$  thin film sandwiched by two Ag layers. To examine the effects of the SPP excitations, the SHG was excited in an attenuated total reflection (ATR) geometry (Kretschmann configuration). Our previous SHG studies of  $\text{Ge}_x(\text{SiO}_2)_{1-x}$  sputter-deposited films<sup>9</sup> demonstrated that the second-order nonlinearity of amorphous  $\text{SiO}_2$  ( $x = 0$ ) films, which vanishes in the electric-dipole approximation due to the centrosymmetric structure (SHG-inactive), can be significantly enhanced by doping Ge into the films to grow  $\text{Ge}_x(\text{SiO}_2)_{1-x}$  ( $x \neq 0$ ) films (SHG-active). To apply this advantageous property of the films to our SHG measurements, we prepared two different MDM samples, one containing a SHG-active  $\text{Ge}_x(\text{SiO}_2)_{1-x}$  layer as the intermediate D layer (GeS-MDM sample) and the other containing a SHG-inactive  $\text{SiO}_2$  layer (S-MDM sample). The SHG intensities obtained for the S-MDM

<sup>a)</sup>s.hayashi@dragon.kobe-u.ac.jp

sample allow us to extract the contribution of the Ag layers from the total SHG intensities of the GeS-MDM sample and further estimate the SHG intensities originating from the  $\text{Ge}_x(\text{SiO}_2)_{1-x}$  layer. We demonstrate that under the SPP excitation conditions, the SHG intensities of the  $\text{Ge}_x(\text{SiO}_2)_{1-x}$  layer embedded in the MDM structure are highly enhanced relative to those of a single  $\text{Ge}_x(\text{SiO}_2)_{1-x}$  layer deposited on a substrate.

## II. EXPERIMENTAL

The MDM structure prepared in this study is schematically shown in Fig. 1(a). First, an Ag thin film  $\sim 30$  nm in thickness was deposited on a fused silica substrate by a vacuum evaporation technique. Then, a  $\text{Ge}_x(\text{SiO}_2)_{1-x}$  thin film was deposited on top of the Ag thin film by an rf magnetron co-sputtering technique described in detail in our previous paper.<sup>9</sup> The value of  $x$  estimated for the present sample is  $\sim 0.07$ . To complete the GeS-MDM sample, another Ag thin film  $\sim 40$  nm in thickness was deposited on top of the  $\text{Ge}_x(\text{SiO}_2)_{1-x}$  thin film. In addition to the GeS-MDM sample, two different reference samples were prepared. One is a similar S-MDM sample containing a pure  $\text{SiO}_2$  thin film as the intermediate D layer. Since  $\text{SiO}_2$  films are SHG-inactive, the SHG signals in the S-MDM sample are generated by the Ag films. The SHG intensities measured for this reference sample are used to estimate the contribution of the Ag thin films to the SHG intensities observed for the GeS-MDM sample. Another reference sample prepared is a single  $\text{Ge}_x(\text{SiO}_2)_{1-x}$  layer deposited on a silica substrate. The deposition of the  $\text{Ge}_x(\text{SiO}_2)_{1-x}$  thin film for this reference sample and the GeS-MDM sample was performed at the same time; therefore, the

thickness and quality of the  $\text{Ge}_x(\text{SiO}_2)_{1-x}$  thin film in these samples are thought to be identical. The SHG enhancement factor (EF) for the  $\text{Ge}_x(\text{SiO}_2)_{1-x}$  layer embedded in the GeS-MDM sample is estimated by dividing its SHG intensity by that of the second reference sample.

We performed angle-scan ATR and SHG measurements in the Kretschmann configuration using the optical setup schematically shown in Fig. 1(b). To perform the angle-scan ATR measurements, the MDM sample was pasted on the bottom surface of a right-angle prism made of a BK7 glass using index matching oil. The prism with the sample was mounted on a computer-controlled rotating stage. A Ti:sapphire femto-second laser with a wavelength of 800 nm (pulse duration of 70 fs, repetition rate of 82 MHz) was used as an excitation source.  $p$ -polarized laser beam was incident on the prism and reflected light was detected by a Si photo-diode. Reflection spectra were obtained by dividing the intensity of the reflected light by that measured for the bare part of the prism. In the ATR measurements, the parallel laser beam which is  $\sim 2$  mm in diameter and 80 mW in power was incident on the prism; the corresponding power density is  $\sim 2.55$  W/cm<sup>2</sup>.

The second-harmonic (SH) light with a wavelength of 400 nm excited by the incident fundamental light in the Kretschmann configuration and exiting from the prism was detected. The reflected SH light was focused on the head of the bundle optical fiber mounted on a rotating arm (detection arm) and guided to the entrance slit of a monochromator equipped with a photomultiplier tube. The SHG intensities were measured by a photon counting method. In the SHG measurements, the incident laser beam of 80 mW was focused on the sample using a lens; the estimated spot size on the sample is  $\sim 0.5$  mm, yielding a power density of  $\sim 40.7$  W/cm<sup>2</sup>. We confirmed that the irradiation with this power density does not cause the damage on the sample. The signal/noise (S/N) ratio in the measurements depends on the total count of photons  $N$  and can be estimated by  $\sqrt{N}$ . To achieve sufficiently high S/N ratios, we used a photon accumulation time of 2 s for the GeS-MDM and S-MDM samples, which yielded S/N ratios that fall in a range between  $\sim 9$  and  $\sim 20$  for various SHG peaks observed. In this paper, the SHG intensities are expressed in terms of photon counts per second (cps) corresponding to the excitation power of 80 mW.

The angle-scan SHG measurements were performed in the following way. First, the angle of incidence  $\theta_{\text{in}}$  of the fundamental light is fixed at an appropriate angle, and the SHG intensity is recorded as a function of the detection angle by rotating the detection arm. The SHG intensity was found to take a maximum value at a certain detection angle. In this work, we define the angle of SHG emission  $\theta_{\text{SHG}}$  as the detection angle that gives the maximum SHG intensity. The maximum SHG intensity measured at  $\theta_{\text{SHG}}$  is recorded as the SHG intensity at the fixed  $\theta_{\text{in}}$ . The SHG intensity obtained in this manner was recorded for various values of  $\theta_{\text{in}}$  scanned in the same angle range as the ATR measurements. The angle-scan SHG spectra measured in this work are thus plotted as a function of  $\theta_{\text{in}}$ . We note here that  $\theta_{\text{SHG}}$  is related to  $\theta_{\text{in}}$  by Eq. (1) given later. The SH light is observed at  $\theta_{\text{SHG}}$  slightly smaller than the angle of specular reflection of the fundamental light as explained in detail later.

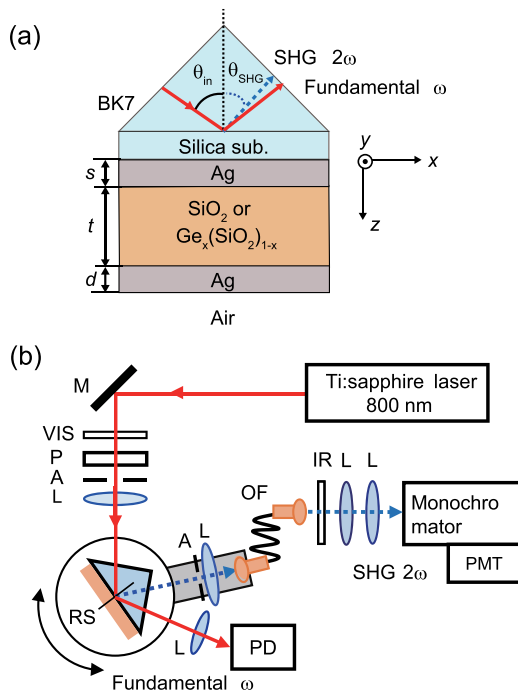


FIG. 1. (a) Multilayer sample attached to a prism (Kretschmann configuration). (b) Optical setup for ATR and SHG measurements. Optical elements used are mirror (M), visible-blocking filter (VIS), polarizer (P), aperture (A), lens (L), bundle optical fiber (OF), and infrared-blocking filter (IR).

For the second reference sample, i.e., a single layer of  $\text{Ge}_x(\text{SiO}_2)_{1-x}$  deposited on the substrate, we measured the transmitted SHG signals and found that the intensity takes a maximum value when the angle of incidence is set at  $50^\circ$ . Since the SHG intensities are found to be very weak compared to those of the GeS-MDM and S-MDM samples, to perform the measurement with a sufficiently large S/N ratio, the incident laser power was set at 160 mW and the photon accumulation time of 10 s was used. With the power used, the incident laser did not cause damage to the sample. The S/N ratio estimated for the maximum intensity is  $\sim 26$ .

### III. RESULTS AND DISCUSSION

#### A. Experimental results

Figures 2(a) and 2(b) show angle-scan ATR spectra obtained for the GeS-MDM and S-MDM samples, respectively. In the spectra, we see two reflectance dips, a sharp dip located at a low angle and a broad one at a high angle. As discussed in detail in our previous papers,<sup>5,6,8</sup> MDM structures can support coupled SPP modes, S-SPP and A-SPP modes, that arise from the coupling between two SPP modes localized at the inner MD interfaces. When the M layers are thin and surrounded by dielectrics, the structure can also support SPP modes localized at the outer MD interfaces. From a comparison with our previous ATR spectra,<sup>6</sup> the sharp dips appearing at  $42.12^\circ$  and  $41.98^\circ$  for the GeS-MDM and S-MDM samples, respectively, can be attributed to the excitation of SPP modes at the Ag/Air interface (Ag/Air-SPP mode). Furthermore, the broad dips appearing at  $55.32^\circ$  and  $48.31^\circ$  can be attributed to the excitation of a symmetric SPP

mode (S-SPP mode). The solid curves shown in Figs. 2(a) and 2(b) are theoretical ATR spectra obtained by electromagnetic (EM) calculations. To calculate the spectra we used a freely available Winspall software package, which allows us to calculate ATR spectra by varying the structural parameters. In the calculation, we assumed a Kretschmann configuration consisting of a BK7 prism, first Ag layer,  $\text{Ge}_x(\text{SiO}_2)_{1-x}$  layer, second Ag layer, and air. We ignored the silica substrate because it can be regarded as a part of the prism. A literature value of the dielectric constant of the BK7 prism at the fundamental wavelength,<sup>10</sup>  $\epsilon_p = 2.283$ , was used. For the GeS-MDM sample, the thicknesses and dielectric constants of the layers used are  $s = 27.8$  nm and  $\epsilon_{\text{Ag}} = -27.25 + i1.651$  for the first Ag layer,  $t = 235$  nm, and  $\epsilon_{\text{GeS}} = 2.900 + i5.790 \times 10^{-3}$  for the  $\text{Ge}_x(\text{SiO}_2)_{1-x}$  layer, and  $d = 39.8$  nm and  $\epsilon_{\text{Ag}} = -29.06 + i1.553$  for the second Ag layer. For the S-MDM sample, the theoretical spectrum was obtained by a set of parameters:  $s = 30.3$  nm and  $\epsilon_{\text{Ag}} = -30.10 + i0.9876$  for the first Ag layer,  $t = 311$  nm and  $\epsilon_{\text{S}} = 2.112$  for the  $\text{SiO}_2$  layer, and  $d = 37.7$  nm and  $\epsilon_{\text{Ag}} = -31.29 + i1.153$  for the second Ag layer. We see that the experimental ATR spectra are very well reproduced by the EM calculations.

Figures 2(c) and 2(d) show angle-scan SHG spectra measured for the GeS-MDM and S-MDM samples, respectively. In the insets, the SHG spectra around the low-angle peaks are compared with the low-angle ATR dips. We see that the peaks in the SHG spectra are located at almost the same angles as the ATR dips seen in Figs. 2(a) and 2(b). The full widths at half maximum (FWHM) of the SHG peaks are also in good agreement with those of the ATR dips. These

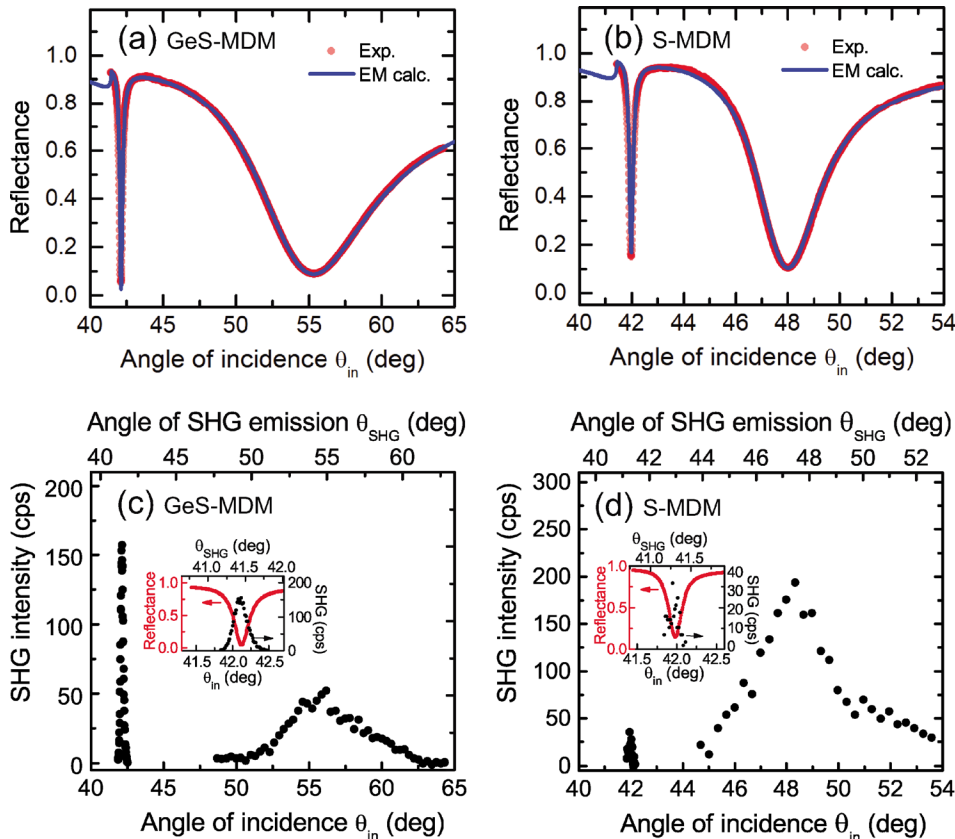


FIG. 2. Experimental and theoretical ATR spectra obtained for GeS-MDM sample (a) and S-MDM sample (b). SHG spectra measured for GeS-MDM sample (c) and S-MDM sample (d). In the insets, low-angle SHG peaks are compared with the low-angle ATR dips appearing in (a) and (b).



features strongly suggest that the low-angle SHG peaks are mediated by the excitation of the Ag/Air-SPP modes, while the high-angle SHG peaks are mediated by the excitation of the S-SPP modes. We found experimentally that the SHG light exits from the prism at an angle slightly smaller than the angle of specular reflection of the fundamental light. Furthermore, we confirmed the following relationship between  $\theta_{\text{in}}$  and  $\theta_{\text{SHG}}$ :

$$\theta_{\text{SHG}} = \sin^{-1} \left[ \left( \frac{n_p^\omega}{n_p^{2\omega}} \right) \sin \theta_{\text{in}} \right], \quad (1)$$

where  $n_p^\omega$  and  $n_p^{2\omega}$  are the refractive index of the prism at the fundamental and SHG wavelengths, respectively. This relationship is a consequence of the conservation of the in-plane wavevector of SH waves subjected to the boundary conditions at the interfaces.<sup>11</sup> Since  $n_p^{2\omega}$  (1.5308, according to Ref. 10) is larger than  $n_p^\omega$  (1.5108, according to Ref. 10),  $\theta_{\text{SHG}}$  becomes smaller than  $\theta_{\text{in}}$ . The upper abscissas in Figs. 2(c) and 2(d) are scaled with  $\theta_{\text{SHG}}$  converted from  $\theta_{\text{in}}$  using Eq. (1).

In a previous SHG study, Teshima *et al.*<sup>7</sup> observed reflection and SHG spectra for their MDM sample consisting of a SHG-inactive PMMA insulator layer sandwiched by two Au layers and reported only one reflection dip and only one SHG peak. In their work, only the S-SPP mode lying in the radiative region (left to the air light line) was excited without using the prism. It should be stressed that our SHG peaks are mediated by the SPP modes lying in the nonradiative region (right to the air light line) observable only in the Kretschmann configuration. We note here that the FWHM of the SHG peaks appearing in Figs. 2(c) and 2(d) are comparable to those of the ATR dips although the SHG peaks are expected to be sharper than the ATR dips because of the quadratic dependence of the SHG intensity on the magnitude of the incident electric field. Naraoka *et al.*<sup>14</sup> have also observed SHG peaks as broad as ATR dips in their previous study of the SHG enhancement in the Kretschmann configuration mediated by the excitation of the SPP mode in Au films even though their theoretical calculations predicted much sharper SHG peaks. The reasons for the broad SHG peaks are not well known at present. However, a lower angular resolution of  $\theta_{\text{in}}$  in the SHG measurements is thought to be one of the reasons. In fact, we used the focused laser beam as the incident light in our SHG experiments, which results in uncertainty in  $\theta_{\text{in}}$  and lowers the angular resolution, while in our ATR experiments, the parallel laser beam was used without focusing it. Scattering of the SH light caused by the inhomogeneity in the bulk of the layers and roughnesses at the interfaces of the multilayer stack may also be the source of the broadening of the SHG peaks.

## B. Estimation of SHG intensities and enhancement factors

According to EM theories of SHG in multilayer systems,<sup>11–15</sup> reflected and transmitted SH light waves are generated in two steps, i.e., excitation and emission steps. In the excitation step, when a fundamental light wave is incident on a multilayer system, due to the reflection and transmission

of waves at the interfaces, waves propagating in the forward and backward directions are generated in each layer, and EM field distributions are established in the system. In a SHG-active layer, a nonlinear polarization, which acts as a source of SH wave, is induced by the fundamental electric field  $\mathbf{E}(\omega)$ ; the second-order nonlinear polarization is expressed as  $\mathbf{P}_{\text{NL}}^{(2)} = \chi^{(2)} : \mathbf{E}(\omega)\mathbf{E}(\omega)$ , where  $\chi^{(2)}$  is a second-order nonlinear susceptibility tensor and the right-hand side of the equation represents a tensorial product with the direct product of  $\mathbf{E}(\omega)$ . In the SH emission process, the SH wave generated by  $\mathbf{P}_{\text{NL}}^{(2)}$  is transmitted to adjacent layers and after multiple reflection and transmission processes at the interfaces, the reflected and transmitted SH waves finally exit from the multilayer system. For a multilayer structure that supports SPP modes, enhanced electric fields near the metallic surfaces can be generated under SPP excitation conditions. When the fundamental electric fields in the SHG-active layer are enhanced, they induce large  $\mathbf{P}_{\text{NL}}^{(2)}$  that enhances in turn the SHG intensity. This is the mechanism of the SHG enhancement in the excitation process that determines the dependence of the SHG intensity on  $\theta_{\text{in}}$ . When the emitted SH light is resonant with a SPP mode at the SH wavelength, we can also expect the SHG enhancement in the SHG emission process. The SHG enhancement in the emission process thus determines the dependence of the SHG intensity on  $\theta_{\text{SHG}}$ . Since the SHG peaks presently observed correlate very well with the ATR dips measured with the fundamental light as demonstrated in Figs. 2(c) and 2(d), the SHG enhancement in the excitation process is thought to play a major role in the present MDM samples. According to our analyses of the SPP dispersion curves (not shown here), at the emission angles of the SHG peaks appearing in Figs. 2(c) and 2(d), the SH light is not resonant with the SPP modes at the SH wavelength. Therefore, large SHG enhancements in the emission process are not anticipated.

We now proceed to estimate the SHG intensity originating from the  $\text{Ge}_x(\text{SiO}_2)_{1-x}$  layer in the GeS-MDM sample and also estimate the SHG EFs. In our S-MDM sample, the  $\text{SiO}_2$  layer is SHG-inactive, while the surfaces and bulk of the Ag layers can be the SHG sources. In contrast, in our GeS-MDM sample, the  $\text{Ge}_x(\text{SiO}_2)_{1-x}$  layer itself is SHG-active and can be the SHG source in addition to the Ag layers. In discussing the SHG intensity resulting from the Ag layers, we follow the arguments developed in previous SHG studies of metallo-dielectric multilayer systems.<sup>14,16,17</sup> In these studies, the SHG signal of the metallic layer is commonly assumed to originate from the surfaces. Furthermore, in the case of generation of *p*-polarized SH light by *p*-polarized fundamental light, it is common to take into account only the  $(z, z, z)$  components of  $\chi^{(2)}$ , where the *z* axis is taken to be normal to the interfaces. In this case, *z* component of the nonlinear polarization  $P_{z,\text{NL}}^{(2)}$  is proportional to  $[E_z(\omega)]^2$  and can be expressed as  $P_{z,\text{NL}}^{(2)} = \chi_{zzz}^{(2)} [E_z(\omega)]^2$ . According to analyses of reflected *p*-polarized SHG originating from the metal surface in the Kretschmann configuration described in Ref. 14, the SH waves are assumed to be plane waves and the SHG intensities are expressed in terms of the Fresnel-transmission and reflection coefficients at the interfaces. For

the discussion of the  $p$ -polarized SHG, it is convenient to use the  $y$  component of the magnetic field  $H_y$  because the magnetic field of the  $p$ -polarized light has only the  $y$  component, where the  $y$  axis is taken to be perpendicular to the plane of incidence of the fundamental wave. Following the arguments developed in Ref. 14, the magnetic field associated with the reflected SH wave generated by a single SHG source and exiting from the prism can be expressed as  $H_y(2\omega) = CF_{\text{em}}(2\omega)\chi_{zzz}^{(2)}[E_z(\omega)]^2$ , where  $C$  is a constant and  $F_{\text{em}}(2\omega)$  is a factor that describes the emission processes including the multiple reflections and refractions of the SH waves at the interfaces, as well as the absorption in the absorbing layers.  $F_{\text{em}}(2\omega)$  is a function of the Fresnel-transmission and reflection coefficients at the SH wavelength and depends on  $\theta_{\text{SHG}}$ . The electric field at the position of the nonlinear source  $E_z(\omega)$  can be related to the incident field  $H_y^{\text{in}}(\omega)$  by  $E_z(\omega) = F_{\text{exc}}(\omega)H_y^{\text{in}}(\omega)$ , where  $F_{\text{exc}}(\omega)$  is a factor that describes the generation of the electric field at the position of the nonlinear source;  $F_{\text{exc}}(\omega)$  is a function of the Fresnel-transmission and reflection coefficients at the fundamental wavelength and depends on  $\theta_{\text{in}}$ .

Since the intensity of the electromagnetic wave is given by the time average of the Poynting vector, the SHG intensity is given by  $I_{\text{SHG}} = A\langle[H_y(2\omega)]^2\rangle$ , where  $A$  is a constant and  $\langle\rangle$  denotes the time average. When  $H_y(2\omega)$  is assumed to be a plane wave, we can simply write as  $I_{\text{SHG}} = \frac{1}{2}A|H_y(2\omega)|^2$ . Using the above expressions for  $H_y(2\omega)$  and  $E_z(\omega)$ , we can write as  $I_{\text{SHG}} = C^2[F_{\text{em}}(2\omega)\chi_{zzz}^{(2)}F_{\text{exc}}(\omega)]^2I_{\text{in}}^2$ , where  $I_{\text{in}}$  is the intensity of the incident light given by  $\frac{1}{2}A|H_y^{\text{in}}(\omega)|^2$ ; this equation is equivalent to Eq. (1) in Ref. 14. When the sample contains more than one SHG source, which is the case for our samples, SH waves generated by different sources are superposed and interfere with each other. Writing the SHG magnetic field generated by the  $j$ th source as  $H_y^j(2\omega)$ , we can express the total SHG intensity as  $I_{\text{SHG}}^{\text{total}} = \frac{1}{2}A|\sum_j H_y^j(2\omega)|^2$ ; the summation is taken over different sources that generate the magnetic field  $H_y^j(2\omega) = CF_{\text{em},j}(2\omega)\chi_{zzz,j}^{(2)}[E_{z,j}(\omega)]^2$ .

The expressions given above suggest that for the discussion of the SHG intensities, it is important to know the distribution of  $E_z(\omega)$  generated inside the multilayer system by the incident light. We performed EM calculations of the electric field distributions associated with the excitations of the Ag/Air- and S-SPP modes. We used a  $2 \times 2$  transfer matrix method together with the structural parameters at the fundamental wavelength mentioned before, which were obtained from the theoretical fit of the experimental ATR spectra. The electric field distributions obtained for the S-MDM and GeS-MDM samples are presented in Figs. 3(a) and 3(b). In the figures,  $|E_z|$  normalized to the amplitude of the incident fundamental wave  $|E_0|$  is plotted as a function of the position  $z$  in the multilayer system; the prism/Ag interface is located at  $z=0$ . The solid curves corresponding to the excitation of the Ag/Air-SPP modes were calculated by setting the angle of incidence at  $\theta_{\text{in}} = 41.98^\circ$  and  $42.12^\circ$ , which correspond to the ATR minimums for the S-MDM and GeS-MDM samples, respectively. The broken curves were obtained with  $\theta_{\text{in}} = 48.31^\circ$  and  $55.32^\circ$ , which are the excitation angles of the S-SPP modes in the S-MDM and GeS-MDM samples, respectively.

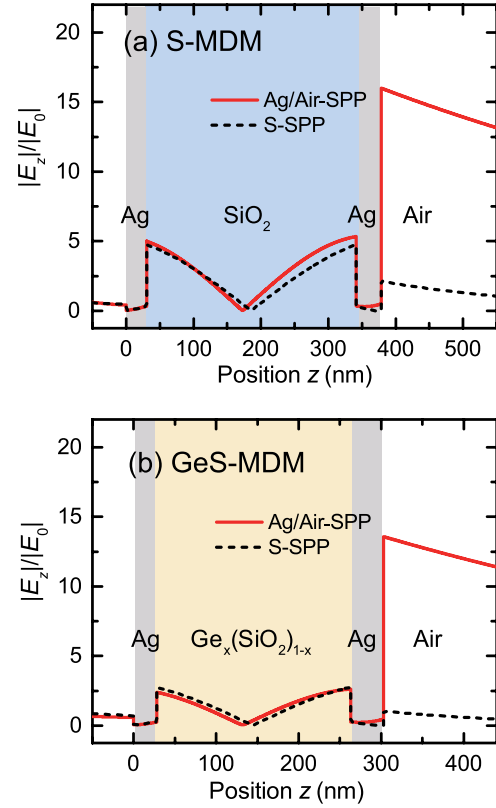


FIG. 3. Electric field profiles calculated for S-MDM sample (a) and GeS-MDM sample (b). The solid and broken curves correspond to excitations of Ag/Air-SPP and S-SPP modes, respectively.

Figures 3(a) and 3(b) suggest that when the Ag/Air-SPP mode is excited, largely enhanced  $E_z$  field is induced at the Ag/Air interface in both the S- and GeS-MDM samples; although  $E_z$  field is discontinuous at the metal/dielectric interface, we take into account the field at the dielectric side because this choice has been proven to be valid in the analyses of the surface SHG of metal layers.<sup>14</sup> At the inner MD and DM interfaces,  $E_z$  fields are also moderately enhanced. Comparing the field distributions for the S- and GeS-MDM samples, we see that  $|E_z|$  values at the interfaces are smaller for the GeS-MDM sample; the smaller values stem from a nonzero imaginary part of the  $\text{Ge}_x(\text{SiO}_2)_{1-x}$  layer. In the GeS-MDM sample,  $|E_z|$  at the Ag/Air interface is smaller by a factor of  $\sim 0.85$ , while at the inner MD and DM interfaces, the  $|E_z|$  values are smaller by factors of  $\sim 0.49$  and  $\sim 0.48$ , respectively. In the case of the S-SPP mode excitation, broken curves in Figs. 3(a) and 3(b) indicate that  $|E_z|$  takes large values at the inner MD interfaces rather than at the Ag/Air interfaces. The values of  $|E_z|$  at the MD, DM, and Ag/Air interfaces in the GeS-MDM sample are smaller than those in the S-MDM samples by factors of 0.50, 0.58, and 0.48, respectively. These factors are used later to estimate the SHG intensities originating from the Ag surfaces in the GeS-MDM sample.

For the GeS-MDM sample, the SHG light observed originates from the SHG-active  $\text{Ge}_x(\text{SiO}_2)_{1-x}$  layer and the Ag layers. Writing the magnetic field of SH wave generated by the  $\text{Ge}_x(\text{SiO}_2)_{1-x}$  layer as  $H_y^{\text{GeS}}$  and a superposition of magnetic fields generated by the SH sources located at the

MD, DM, and Ag/Air interfaces as  $H_y^{\text{Ag}} (= H_{y,\text{MD}}^{\text{Ag}} + H_{y,\text{DM}}^{\text{Ag}} + H_{y,\text{Ag/Air}}^{\text{Ag}})$ , we can express the SHG intensity observed for the GeS-MDM sample as  $I_{\text{GeS}}^{\text{total}} = \frac{1}{2}A|H_y^{\text{GeS}} + H_y^{\text{Ag}}|^2$ . When the phase difference  $\delta$  between the two fields is introduced, we have  $I_{\text{GeS}}^{\text{total}} = I_{\text{GeS}}^{\text{GeS}} + I_{\text{GeS}}^{\text{Ag}} + 2\sqrt{I_{\text{GeS}}^{\text{GeS}}}\sqrt{I_{\text{GeS}}^{\text{Ag}}}\cos\delta$ , where  $I_{\text{GeS}}^{\text{GeS}}$  and  $I_{\text{GeS}}^{\text{Ag}}$  are given by  $\frac{1}{2}A|H_y^{\text{GeS}}|^2$  and  $\frac{1}{2}A|H_y^{\text{Ag}}|^2$ , respectively. The constructive and destructive interferences result in  $\cos\delta = \pm 1$  and consequently,  $I_{\text{GeS}}^{\text{total}}$  falls in a range given by  $(\sqrt{I_{\text{GeS}}^{\text{GeS}}} - \sqrt{I_{\text{GeS}}^{\text{Ag}}})^2 \leq I_{\text{GeS}}^{\text{total}} \leq (\sqrt{I_{\text{GeS}}^{\text{GeS}}} + \sqrt{I_{\text{GeS}}^{\text{Ag}}})^2$ . Rewriting this relation for  $I_{\text{GeS}}^{\text{GeS}}$ , under the condition  $I_{\text{GeS}}^{\text{GeS}} > I_{\text{GeS}}^{\text{Ag}}$ , which can be justified from the experimental data presented in Figs. 2(c) and 2(d), we finally obtain an important relation written as

$$I_{\text{LB}}^{\text{GeS}} \leq I_{\text{GeS}}^{\text{GeS}} \leq I_{\text{UB}}^{\text{GeS}}, \quad (2)$$

with,

$$I_{\text{LB}}^{\text{GeS}} = \left( \sqrt{I_{\text{GeS}}^{\text{total}}} - \sqrt{I_{\text{GeS}}^{\text{Ag}}} \right)^2, \quad (3)$$

and

$$I_{\text{UB}}^{\text{GeS}} = \left( \sqrt{I_{\text{GeS}}^{\text{total}}} + \sqrt{I_{\text{GeS}}^{\text{Ag}}} \right)^2. \quad (4)$$

The experimental values of  $I_{\text{GeS}}^{\text{total}}$  are available from Fig. 2(c). Therefore, values of the lower bound  $I_{\text{LB}}^{\text{GeS}}$  and the upper bound  $I_{\text{UB}}^{\text{GeS}}$  can be obtained from those of  $I_{\text{GeS}}^{\text{Ag}}$ .

$I_{\text{GeS}}^{\text{Ag}}$  cannot be obtained directly from the SHG data on the GeS-MDM sample. In this work, we thus attempt to estimate  $I_{\text{GeS}}^{\text{Ag}}$  from the SHG intensity observed for the S-MDM sample  $I_{\text{S}}^{\text{Ag}}$ . To do so, we derive a relation that connects  $I_{\text{GeS}}^{\text{Ag}}$  to  $I_{\text{S}}^{\text{Ag}}$ . The SHG intensity of the S-MDM sample originates only from the Ag layers and can be written in terms of a superposition of the magnetic fields of SH waves generated by the sources located at the MD, DM, and Ag/Air interfaces as  $I_{\text{S}}^{\text{Ag}} = \frac{1}{2}A|H_{y,\text{MD}}^{\text{S,Ag}} + H_{y,\text{DM}}^{\text{S,Ag}} + H_{y,\text{Ag/Air}}^{\text{S,Ag}}|^2$ . As mentioned before, the SHG magnetic fields generated by different sources are expressed in the form of  $H_y^i(2\omega) = CF_{\text{em},j}(2\omega)\chi_{zzz,j}^{(2)}[E_{z,j}(\omega)]^2$  and determined by three factors  $F_{\text{em},j}(2\omega)$ ,  $\chi_{zzz,j}^{(2)}$ , and  $[E_{z,j}(\omega)]^2$ . We have already noted that the theoretical results presented in Figs. 3(a) and 3(b) allow us to determine the ratios of  $[E_{z,j}(\omega)]^2$  at the MD, DM, and Ag/Air interfaces in the GeS-MDM sample to those in the S-MDM sample. The factors  $F_{\text{em},j}(2\omega)$  and  $\chi_{zzz,j}^{(2)}$  for the GeS-MDM sample are thought to be modified from those in the S-MDM sample because the transparent  $\text{SiO}_2$  layer is replaced by the absorbing  $\text{Ge}_x(\text{SiO}_2)_{1-x}$  layer and the structural parameters (thicknesses and dielectric constants) are not the same for the two samples. However, detailed analyses on the modifications of these factors are difficult at present due partly to the lack of experimental values of  $\chi_{zzz,j}^{(2)}$  at the interfaces and the optical constants of the layers at the SH wavelength. Therefore, we content ourselves with performing semiquantitative estimations of  $I_{\text{GeS}}^{\text{Ag}}$  under an assumption that the factors  $F_{\text{em},j}(2\omega)$  and  $\chi_{zzz,j}^{(2)}$  for the GeS-MDM sample are not changed from those for the S-MDM sample. We take into account only the decrease in  $[E_{z,j}(\omega)]^2$  in the GeS-MDM sample.

We already noted that under the excitation of the Ag/Air-SPP mode,  $|E_z|$  values at the MD, DM, and Ag/Air interfaces in the GeS-MDM sample become smaller compared to those in the S-MDM sample by factors of  $\sim 0.49$ ,  $\sim 0.48$ , and  $\sim 0.85$ , respectively. Under the excitation of the S-SPP mode, the factors are 0.50, 0.58, and 0.48, respectively. In the case of the excitation of the Ag/Air-SPP mode, the magnetic fields of the SH waves generated at the MD, DM, and Ag/Air interfaces in the GeS-MDM sample are thus given by  $H_{y,\text{MD}}^{\text{Ag}} = 0.49^2 H_{y,\text{MD}}^{\text{S,Ag}}$ ,  $H_{y,\text{DM}}^{\text{Ag}} = 0.48^2 H_{y,\text{DM}}^{\text{S,Ag}}$ , and  $H_{y,\text{Ag/Air}}^{\text{Ag}} = 0.85^2 H_{y,\text{Ag/Air}}^{\text{S,Ag}}$ , respectively. Therefore, the contribution of the Ag layers to the SHG intensity of the GeS-MDM sample can be estimated by  $I_{\text{GeS}}^{\text{Ag}} = \frac{1}{2}A|0.49^2 H_{y,\text{MD}}^{\text{S,Ag}} + 0.48^2 H_{y,\text{DM}}^{\text{S,Ag}} + 0.85^2 H_{y,\text{Ag/Air}}^{\text{S,Ag}}|^2$ . Without loss of generality, we can set as  $I_{\text{GeS}}^{\text{Ag}} < \frac{1}{2}A|0.85^2 (H_{y,\text{MD}}^{\text{S,Ag}} + H_{y,\text{DM}}^{\text{S,Ag}} + H_{y,\text{Ag/Air}}^{\text{S,Ag}})|^2 = 0.85^4 I_{\text{S}}^{\text{Ag}} = 0.52 I_{\text{S}}^{\text{Ag}}$ . In the case of the excitation of the S-SPP mode, repeating the same argument, we can set as  $I_{\text{GeS}}^{\text{Ag}} < 0.58^4 I_{\text{S}}^{\text{Ag}} = 0.11 I_{\text{S}}^{\text{Ag}}$ . From these relations, the upper bounds of  $I_{\text{GeS}}^{\text{Ag}}$  are found to be  $I_{\text{GeS}}^{\text{Ag}+} = 0.52 I_{\text{S}}^{\text{Ag}}$  and  $0.11 I_{\text{S}}^{\text{Ag}}$  for the excitations of the Ag/Air- and S-SPP modes, respectively. In the following estimations, we use values of  $I_{\text{GeS}}^{\text{Ag}+}$  in place of  $I_{\text{GeS}}^{\text{Ag}}$ .

The value of  $I_{\text{S}}^{\text{Ag}}$  can be obtained from the experimental data presented in Fig. 2(d) and can be converted into that of  $I_{\text{GeS}}^{\text{Ag}+}$ . The experimental value of  $I_{\text{GeS}}^{\text{total}}$  can be read from Fig. 2(c). Therefore, inserting these values into Eqs. (3) and (4), we can obtain values of  $I_{\text{LB}}^{\text{GeS}}$  and  $I_{\text{UB}}^{\text{GeS}}$ . In the case of the excitation of the Ag/Air-SPP mode, multiplying 0.52 by the SHG peak intensity in the S-MDM sample ( $I_{\text{S}}^{\text{Ag}}$ ) found in the inset of Fig. 2(d) ( $\sim 36$  cps), we obtain  $I_{\text{GeS}}^{\text{Ag}+} \sim 19$  cps. On the other hand, the SHG peak intensity  $I_{\text{GeS}}^{\text{total}}$  upon Ag/Air-SPP excitation is 158 cps as found in the inset of Fig. 2(c). Inserting these values into Eqs. (3) and (4), we obtain  $67.4 \text{ cps} < I_{\text{GeS}}^{\text{GeS}} < 289 \text{ cps}$ . In the case of the excitation of the S-SPP mode, values of  $I_{\text{S}}^{\text{Ag}}$  and  $I_{\text{GeS}}^{\text{total}}$  read from Fig. 2(d) and 2(c) are  $\sim 195$  and 53 cps, respectively. Multiplying 0.11 by the value of  $I_{\text{S}}^{\text{Ag}} = 195$  cps, we obtain  $I_{\text{GeS}}^{\text{Ag}+} \sim 22$  cps. From Eqs. (3) and (4), it follows that  $6.7 \text{ cps} < I_{\text{GeS}}^{\text{GeS}} < 143 \text{ cps}$ . In the present estimations, we neglected the absorption of the SH light inside the  $\text{Ge}_x(\text{SiO}_2)_{1-x}$  layer. Among others, the negligence of the absorption is thought to be the most serious source of errors in the estimations. The absorption may decrease the values of  $I_{\text{GeS}}^{\text{Ag}+}$ . Smaller values of  $I_{\text{GeS}}^{\text{Ag}+}$  increase the estimated values of  $I_{\text{LB}}^{\text{GeS}}$  and decrease those of  $I_{\text{UB}}^{\text{GeS}}$ . Therefore,  $I_{\text{GeS}}^{\text{GeS}}$  is expected to fall into narrower intervals. This means that the above relations for  $I_{\text{GeS}}^{\text{GeS}}$  are still valid, even when the absorption is included in the estimation.

To obtain experimental SHG EFs, we measured the SHG intensity of the second reference sample, i.e., a single layer of  $\text{Ge}_x(\text{SiO}_2)_{1-x}$  deposited on the substrate. We measured the transmitted SHG signals and found that the intensity takes a maximum value at an angle of incidence of  $50^\circ$ ; the maximum intensity obtained was 1.69 cps. Dividing the estimated SHG intensities given above by this reference value, we finally obtain  $39.9 < \text{EF} < 171$  for the SHG mediated by the Ag/Air-SPP mode and  $3.96 < \text{EF} < 84.6$  for the SHG mediated by the S-SPP mode, respectively. As mentioned above, when the absorption of the SH light inside the  $\text{Ge}_x(\text{SiO}_2)_{1-x}$  layer is taken into account, estimated EFs are



expected to fall into narrower intervals. To fully explain the present experimental results, calculations that take into account the changes in the factors  $F_{\text{em},j}(2\omega)$  and  $\chi_{zzz,j}^{(2)}$  are required. For this purpose, the experimental determinations of  $\chi_{zzz,j}^{(2)}$  and the optical constants at the SH wavelength are also required.

#### IV. CONCLUSION

In conclusion, we have experimentally demonstrated that the SHG intensities originating from the  $\text{Ge}_x(\text{SiO}_2)_{1-x}$  layer embedded in the MDM structure are enhanced relative to that from the single  $\text{Ge}_x(\text{SiO}_2)_{1-x}$  layer. The present SHG enhancement is mainly caused by the enhancement of the fundamental electric fields upon excitations of the Ag/Air-SPP and S-SPP modes in the Kretschmann configuration. Since the SHG intensity observed for the GeS-MDM sample is the superposition of the contributions from the Ag layers and the  $\text{Ge}_x(\text{SiO}_2)_{1-x}$  layer, the SHG intensity observed for the S-MDM sample, which contains only the contribution from the Ag layers, was used to extract the contribution from the  $\text{Ge}_x(\text{SiO}_2)_{1-x}$  layer. Detailed analyses of the experimental results allowed us to estimate the upper and lower bounds of the SHG EF. Our estimations indicate that  $39.9 < \text{EF} < 171$  in the case of the Ag/Air-SPP excitation and  $3.96 < \text{EF} < 84.6$  in the case of the S-SPP excitation. Although the electromagnetic modes excited in the MDM structure are plasmonic in nature, they have characteristics of the waveguide modes, being accompanied by the distributions of large electric fields concentrated inside the D layer. The SHG enhancements demonstrated in the present study may pave new avenue for developing waveguide devices based on SHG-active dielectric layers, in particular C-MOS compatible amorphous layers.

#### ACKNOWLEDGMENTS

We would like to thank A. Kitao for helpful discussions. This work was supported in part by JSPS KAKENHI Grant Nos. 16K04979 and 16H03828.

- <sup>1</sup>H. J. Simon, D. E. Mitchell, and J. G. Watson, "Optical second-harmonic generation with surface plasmons in silver films," *Phys. Rev. Lett.* **33**, 1531 (1974).
- <sup>2</sup>M. Kauranen and A. V. Zayats, "Nonlinear plasmonics," *Nat. Photonics* **6**, 737 (2012).
- <sup>3</sup>J. Butet, P. F. Brevet, and O. J. F. Martin, "Optical second harmonic generation in plasmonic nanostructures: From fundamental principles to advanced applications," *ACS Nano* **9**, 10545 (2015).
- <sup>4</sup>E. N. Economou, "Surface plasmons in thin films," *Phys. Rev.* **182**, 539 (1969).
- <sup>5</sup>S. Hayashi and T. Okamoto, "Plasmonics: Visit the past to know the future," *J. Phys. D: Appl. Phys.* **45**, 433001 (2012).
- <sup>6</sup>S. Refki, S. Hayashi, A. Rahmouni, D. V. Nesterenko, and Z. Sekkat, "Anticrossing behavior of surface plasmon polariton dispersions in metal-insulator-metal structures," *Plasmonics* **11**, 433 (2016).
- <sup>7</sup>D. Teshima, R. Fujimura, and K. Kajikawa, "Resonant second-harmonic generation in metal-insulator-metal structure," *Jpn. J. Appl. Phys., Part 1* **53**, 32202 (2014).
- <sup>8</sup>S. Hayashi, A. Maekawa, S. C. Kim, and M. Fujii, "Mechanism of enhanced light emission from an emitting layer embedded in metal-insulator-metal structures," *Phys. Rev. B* **82**, 35441 (2010).
- <sup>9</sup>I. Kawamura, K. Imakita, M. Fujii, and S. Hayashi, "Second harmonic generation from Ge doped  $\text{SiO}_2$  ( $\text{Ge}_x(\text{SiO}_2)_{1-x}$ ) thin films grown by sputtering," *Appl. Phys. Lett.* **103**, 201117 (2013).
- <sup>10</sup>M. N. Polyanskiy, see <http://refractiveindex.info/> for "Refractive index database" (2015).
- <sup>11</sup>N. Bloembergen and P. S. Pershan, "Light waves at the boundary of nonlinear media," *Phys. Rev.* **128**, 606 (1962).
- <sup>12</sup>W. N. Herman and L. M. Hayden, "Maker fringes revisited: Second-harmonic generation from birefringent or absorbing materials," *J. Opt. Soc. Am. B* **12**, 416 (1995).
- <sup>13</sup>W. S. Kolthammer, D. Barnard, N. Carlson, A. D. Edens, N. A. Miller, and P. N. Saeta, "Harmonic generation in thin films and multilayers," *Phys. Rev. B* **72**, 45446 (2005).
- <sup>14</sup>R. Naraoka, H. Okawa, K. Hashimoto, and K. Kajikawa, "Surface plasmon resonance enhanced second-harmonic generation in Kretschmann configuration," *Opt. Commun.* **248**, 249 (2005).
- <sup>15</sup>D. H. Park and W. N. Herman, "Closed-form maker fringe formulas for poled polymer thin films in multilayer structures," *Opt. Express* **20**, 173 (2012).
- <sup>16</sup>G. D'Aguzzo, M. C. Larciprete, N. Mattiucci, A. Belardini, M. J. Bloemer, E. Fazio, O. Buganov, M. Centini, and C. Sibilia, "Experimental study of Bloch vector analysis in nonlinear, finite, dissipative systems," *Phys. Rev. A* **81**, 013834 (2010).
- <sup>17</sup>N. Mattiucci, G. D'Aguzzo, and M. Bloemer, "Second harmonic generation from metallo-dielectric multilayered structures in the plasmonic regime," *Opt. Express* **18**, 23698 (2010).